Journal of Alloys and Compounds 509 (2011) 87–93

Contents lists available at ScienceDirect

Journal of Alloys and Compounds

journal homepage: www.elsevier.com/locate/jallcom

Investigation of some physical properties of Gd added Bi-2223 superconductors

C. Terzioglu *

Department of Physics, Faculty of Arts and Science, Abant Izzet Baysal University, 14280 Bolu, Turkey

ARTICLE INFO

Article history:
Received 4 November 2009
Received in revised form 12 August 2010
Accepted 26 August 2010

Keywords:
Gd addition
Microhardness
Indentation size effect
Kick's law
MPSR model and HK model

ABSTRACT

X-ray powder diffraction (XRD), scanning electron microscopy (SEM), dc electrical resistivity, critical current density and static microindentation measurements are performed to investigate some physical properties of $Bi_{1.8}Pb_{0.35}Sr_{1.9}Ca_{2.1}Cu_3Gd_xO_y$ superconducting samples with $x = 0.0$, 0.1, 0.3 and 0.5. We observe from the transport measurements that, for the Gd added sample, the critical transition temperature (T_c) and the critical current density (J_c) are decreased in comparison with that of undoped sample. In addition, surface morphology and grain connectivity of the samples are degraded and the high-T_c phase of the samples decreases with increasing Gd addition. The indentation load versus diagonal length of the samples under different indentation loads in the range of 0.245–2.940 N are measured. The microindentation measurements showed that, for the Gd added sample, the load dependent (apparent) microhardness value (H_v) is lower in comparison with that of the pure sample ($x = 0$). The values of H_v are found to be load dependent. In addition, we extract the load independent (true) microhardness using the Kick's law, proportional specimen resistance (PSR), modified proportional specimen resistance (MPSR) and the Hays–Kendall (HK) approach and compare the true hardness with the apparent hardness. The possible reasons for the observed degradation in microstructure, superconducting and mechanical properties due to Gd addition are discussed.

1. Introduction

Indentation microhardness measurement is a convenient method to investigate the mechanical properties of a small volume of specimens. The conventional procedure of hardness measurement consists of applying a fixed load on a diamond indenter and measuring the dimension of the resultant indentation on the surface of the specimen. Investigations on hardness measurements have confirmed that load dependent hardness of a given specimen is a function of the applied load [1,2]. The Vickers microhardness (apparent) values of different applied loads can be calculated using the relation

$$H_v = 1854.4\left(\frac{F}{d^2}\right) \quad \text{(GPa)} \tag{1}$$

where F is the applied load in N and d is the diagonal length of the indentation mark in μm. It is expected that the indenter makes geometrically similar indentation; hence it follows that the measured hardness must be independent of the applied load. However, it has been well known that microhardness calculated using Eq. (1) is load dependent for many materials. In general, higher applied loads lead to lower hardness values. The reason for this behavior is explained by Khalil [3] as follows: a) at larger indention loads, the Vickers hardness is found to be small which might be due to the presence of weak grain boundaries of the superconducting ceramics; b) at smaller indention loads, the Vickers hardness is higher which can be ascribed to the fact that measured hardness values were more indicative of the monocrystalline state without interference from grain boundaries. A non-linear hardness versus load behavior has been observed in the literature for Bi-2223 and Bi-2212 [3–7] and for MgB_2 superconductors [8,9], and is known as the indentation size effect (ISE).

In order to analyze the ISE behavior and to estimate the true microhardness value, several relationships between the applied load and the resulting indentation size has been suggested [1,10–12]. One of those relations is known as Meyer's law and can be expressed as [2,13,14]

$$F = Kd^n \tag{2}$$

where the power n is the Meyer number, and K is the standard hardness constant. When $n = 2$, the hardness is independent of the applied load and is given by Kick's law

$$F = Kd^2 \tag{3}$$

Kick's law is hardly met for many materials because the exponent n is not equal to 2 in most cases. Meyer's law generally provides a satisfactory description for the experimental data for most of the

* Tel.: +90 374 254 1285; fax: +90 374 253 4642.
E-mail address: terioglu_c@ibu.edu.tr.

0925-8388/$ – see front matter © 2010 Elsevier B.V. All rights reserved.
doi:10.1016/j.jallcom.2010.08.105

materials but cannot provide any explanation for the origin of the observed ISE [1,10,15].

It has been well known that the elastic recovery would occur in the vicinity of the indentation impression after the indenter is removed so that the indentation size would shorten to a certain degree [16]. In order to estimate the true hardness, H_0, an elastic component, d_e, should be added to the measured plastic indentation semidiagonal, d_p [17]. This result is given by

$$H_0 = 1854.4\frac{F}{(d_p + d_e)^2} \quad (\text{GPa}) \tag{4}$$

The slope of the graph of measured indentation diagonals versus the square root of the applied load gives $(H_0)^{-1/2}$ while its vertical intercept provides the elastic part of the indentation semidiagonal, d_e.

The proportional specimen resistance (PSR) model is another approach used recently to investigate the ISE behavior of various materials [3,7,9,18]. According to the PSR model, ISE behavior is governed by

$$\frac{F}{d} = K_1 + K_2 d \tag{5}$$

where the coefficients K_1 and K_2 are the load dependent hardness and the load independent hardness, respectively [9]. Based on the PSR model, for the microindentation test with a Vickers indenter, true hardness, H_{PSR}, can be determined directly by the relation [9]

$$H_{PSR} = 1854.4K_2 \quad (\text{GPa}) \tag{6}$$

In order to account for the effect of the machining-induced plastically deformed surface on the microhardness measurements, it was proposed that the PSR model should be modified as [1]

$$F = K_3 + K_4 d + K_5 d^2 \tag{7}$$

where K_3 corresponds to the minimum applied load to produce an indentation. K_4 and K_5 in this formula are related to energy dissipated in creating a new surface of unit area and in producing a permanent deformation of unit volume, respectively. K_5 is a measure of the load independent hardness estimated by the modified proportional specimen resistance (MPSR) model. It should be noted that the K_1 and K_2 constants in Eq. (5) are the same as K_4 and K_5 in Eq. (7). According to the MPSR model, the load independent (true) hardness, H_{MPSR}, can be calculated by Eq. (6).

In order to examine the ISE behavior, Hays and Kendall (HK) [11] proposed that there exist minimum levels of the applied test load, $F_{0\,HK}$, called minimum applied load to produce an indentation. They introduced an effective indentation load, $F_{eff} = F - F_{0\,HK}$, and proposed the following relationship (modified Kick's law),

$$F - F_{0\ HK} = K_6 d^2 \tag{8}$$

where K_6 is the load independent hardness constant calculated by HK approach for a given sample. According to the HK approximation, load independent microhardness, H_{HK}, can be calculated as

$$H_{HK} = 1854.4K_6 \quad (\text{GPa}) \tag{9}$$

Extensive substitution and doping studies have been carried out on Bi-based high-T_c superconductors in order to improve their microstructure, mechanical and superconducting properties and to explain the mechanism of superconductivity [7,19–22]. In previous studies [18,23], we investigated the effect of Gd addition on the mechanical and superconducting properties of the samples that are used in the present study. Mechanical (microhardness, Young's modulus, yield strength and fracture toughness) and superconducting properties of the samples are found to depend on the amount of Gd addition. The Gd addition was found to degrade the microstructure, superconducting and mechanical properties of $Bi_{1.8}Pb_{0.35}Sr_{1.9}Ca_{2.1}Cu_3Gd_xO_y$.

The aim of the present work is to present some experimental data on the superconducting, microstructure and microindentation hardness of the Gd added Bi-2223 samples and then, to analyze the observed ISE behavior based on various models proposed in the literature. The load dependence of microhardness is a result of experimental techniques used to measure it. One would hope to isolate load independent microhardness using several models that are developed to understand the load–microhardness relation.

2. Experimental details

The Gd added $Bi_{1.8}Pb_{0.35}Sr_{1.9}Ca_{2.1}Cu_3Gd_xO_y$ samples ($x = 0.0$, 0.1, 0.3, and 0.5) were prepared by the standard solid-state reaction method using high purity chemicals Bi_2O_3 (99.99%), PbO (99.9+%), $SrCO_3$ (99.9+%), $CaCO_3$ (99+%), CuO (99+%) and Gd_2O_3 (99+%) [18]. These oxides and carbonates were weighed and mixed in a grinding machine for 24 h. After milling, the mixed powders were subjected to a three-stage calcination process in air at different temperatures (700, 750 and 800 °C) for 24 h. Following every calcination stage at these temperatures, the mixture was cooled to room temperature and ground. After completing the process, the powder material was pelletized into rectangular bars of 10 mm × 4 mm × 2 mm at 300 MPa. The pellets were sintered in air at 830 °C for 48 h and then cooled down to room temperature. The heating and cooling rates were chosen to be 10 and 3 °C min^{-1}, respectively. The calcinations and annealing processes of the samples were carried out using a programmable tube furnace (PROTHERM-Model PTF 12/75/200). For comparison, an undoped sample was also annealed under the same conditions. The samples annealed at 830 °C for 48 h with different Gd additions of $x = 0.0$, 0.1, 0.3, and 0.5 in $Bi_{1.8}Pb_{0.35}Sr_{1.9}Ca_{2.1}Cu_3Gd_xO_y$ will be hereafter denoted as Gd0, Gd1, Gd3, and Gd5, respectively.

Narrow rectangular pieces were cut out from the pellets. We measured temperature dependence (40–130 K) of resistivity of these strips using four-point contact technique with 5 mA dc current in a cryostat. The transition temperature T_c was determined as the temperature at zero resistivity. Room temperature resistivities were calculated from *I–V* curves at room temperature. The critical current density J_c was determined from the current–voltage characteristics of the samples at 77 K. The critical current I_c was determined at the onset of a voltage with a criterion of 1 μV/cm, and the J_c was obtained from I_c and the cross-sectional area of the samples. We only measured the critical current density value for Gd0 and Gd1 samples since Gd3 and Gd5 samples are not superconductors at 77 K.

The phase analysis of the samples was done using a Rigaku D/Max-IIIC diffractometer with CuK_α radiation in the range $2\theta = 4$–60° with a scan speed of 3°/min and a step increment of 0.02° at room temperature. These XRD patterns were obtained from the surface of the bulk samples. The phase ratio and lattice parameters were determined from these XRD patterns.

Microstructural examination of the samples was taken from fracture surfaces of the bulk samples using a JEOL 6390-LV scanning electron microscope. The surface morphologies of the samples were studied using a SEM in combination with an energy dispersive X-ray spectrometer (EDS). The EDS analysis was used for studying the chemical composition of the samples. Hardness measurements of $Bi_{1.8}Pb_{0.35}Sr_{1.9}Ca_{2.1}Cu_3Gd_xO_y$ samples were performed on the polished surface of the examined samples with a digital microhardness tester (Instron Series 2100) at room temperature. All samples were polished prior to being tested. The applied load, *F*, was varied from 0.245 to 2.940 N and the applied time was 10 s for all trials, and the diagonals of indentation were measured with an accuracy of ±0.1 μm. Indentations were made at different parts of the samples' surface in such a way that the distance between any two indentations was not less than two times the diagonal of the indentation mark to avoid surface effects due to neighboring indentation. An average of 5 readings at different locations of the specimen surfaces was taken to obtain reasonable mean values for each load.

3. Results and discussion

3.1. Microstructure and transport properties

In order to investigate the relationship between the mechanical properties and the microstructure, and the transport properties of the samples, we have performed XRD, SEM, EDS, dc electrical resistivity and critical current density measurements.

Fig. 1 shows the X-ray powder diffraction patterns for all the samples. Open circles (○), stars (⋆), and (&) in this figure indicate the low-T_c, high-T_c and Ca_2PbO_4 phases, respectively. The calculated phase ratio, and lattice parameters *a* and *c* for high-T_c and low-T_c phases are tabulated in Table 1. The lattice parameter *a* in the low-T_c phase increases from 5.415 to 5.466 Å while the lattice

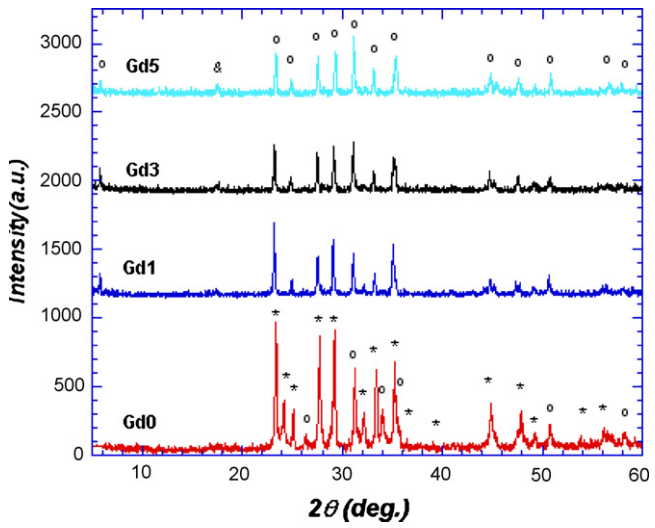

Fig. 1. XRD patterns of the (a) Gd0, (b) Gd1, (c) Gd3 and (d) Gd5 samples.

parameter c decreases from 30.715 to 30.550 Å with increasing Gd content. However, the lattice parameter a in the high-T_c phase is estimated to be 5.416 and 5.420 Å while the lattice parameter c is estimated to be 37.206 and 37.165 Å for the Gd0 and Gd1 samples, respectively. The most important findings from the XRD patterns depicted in Fig. 1 is an increase in the ratio of low-T_c (Bi-2212) to the high-T_c (Bi-2223) phase as Gd-doping is increased. For the Gd3 and Gd5 samples Bi-2223 phase is completely absent. Thus, XRD results indicate that Gd-doping favours the formation of Bi-2212 phase. It is also found that the peak intensity decreases with higher Gd concentration. (0 0 2)L peak and Ca_2PbO_4 impurity peak exist in the Gd-doped samples while they are absent in Gd0 sample. The lattice parameter a (c) is found to increase (decrease) with increasing Gd content.

Fig. 2 exhibits the SEM images of the fracture surface morphology of the samples. The grain size of the Gd0 sample is relatively larger than that of the Gd added samples. The Gd5 sample has non-uniform surface with smaller grains, voids and signs of partial melting on its micrograph. Based on those images, it can be stated that grain size and texturing decrease with increasing Gd-doping. The decrease in grain size with Gd addition suggests that the doping element acts as a growth inhibitor which limits the grain size [24]. Images also indicate that Gd addition has a negative effect on the surface morphology and grain connectivity of $Bi_{1.8}Pb_{0.35}Sr_{1.9}Ca_{2.1}Cu_3O_y$. We have performed EDS measurements for elemental analysis as presented in Fig. 3. As can be seen from the figure, it was observed that the added Gd is distributed in the Gd added samples and the percentage of Gd is low in the Gd1 sample and it increases with increasing Gd addition.

We have measured the resistivity as a function of temperature to determine T_c in the range 40–130 K. Fig. 4 displays the measured resistivity and derivative resistivity as a function of temperature.

Table 1
Some characteristics of superconducting samples.

Samples	T_c^{offset} (K)	Volume fraction (%)		a (Å)	c (Å)	Resistivity at 300 K (mΩ cm)
		2212	2223			
Gd0	105 ± 0.2	08	92	5.416 (2223)5.415 (2212)	37.206 (2223)30.715 (2212)	2.456
Gd1	80 ± 0.2	30	70	5.432 (2223)5.422 (2212)	37.165 (2223)30.702 (2212)	2.829
Gd3	62 ± 0.2	100	–	5.440(2212)	30.589 (2212)	6.321
Gd5	42 ± 0.2	100	–	5.466 (2212)	30.550 (2212)	11.639

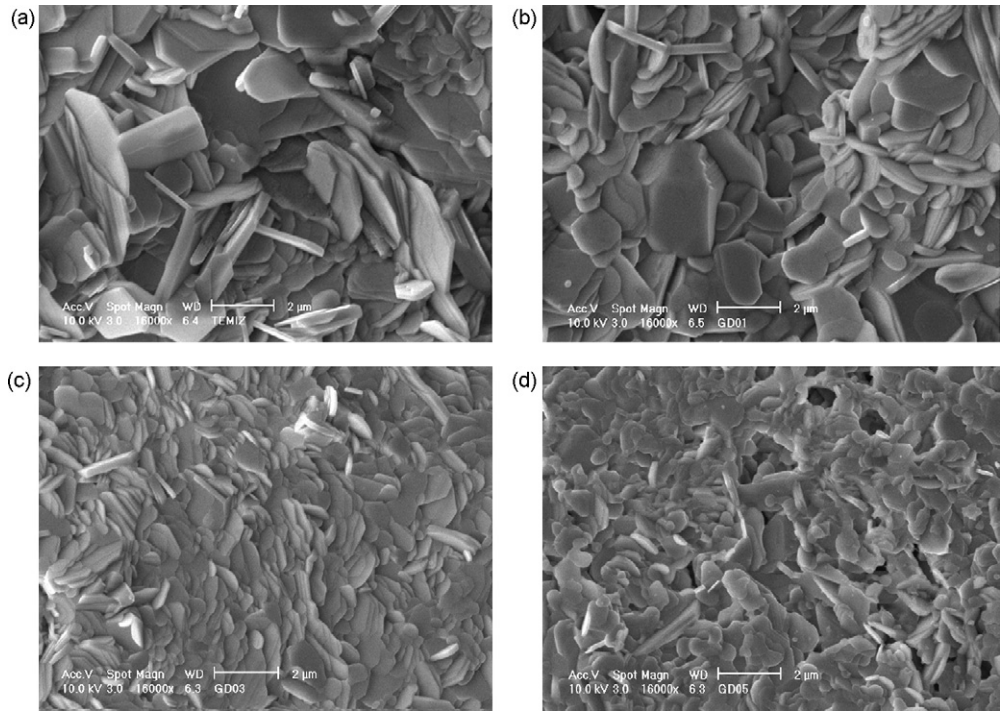

Fig. 2. SEM micrographs of the (a) Gd0, (b) Gd1, (c) Gd3 and (d) Gd5 samples.

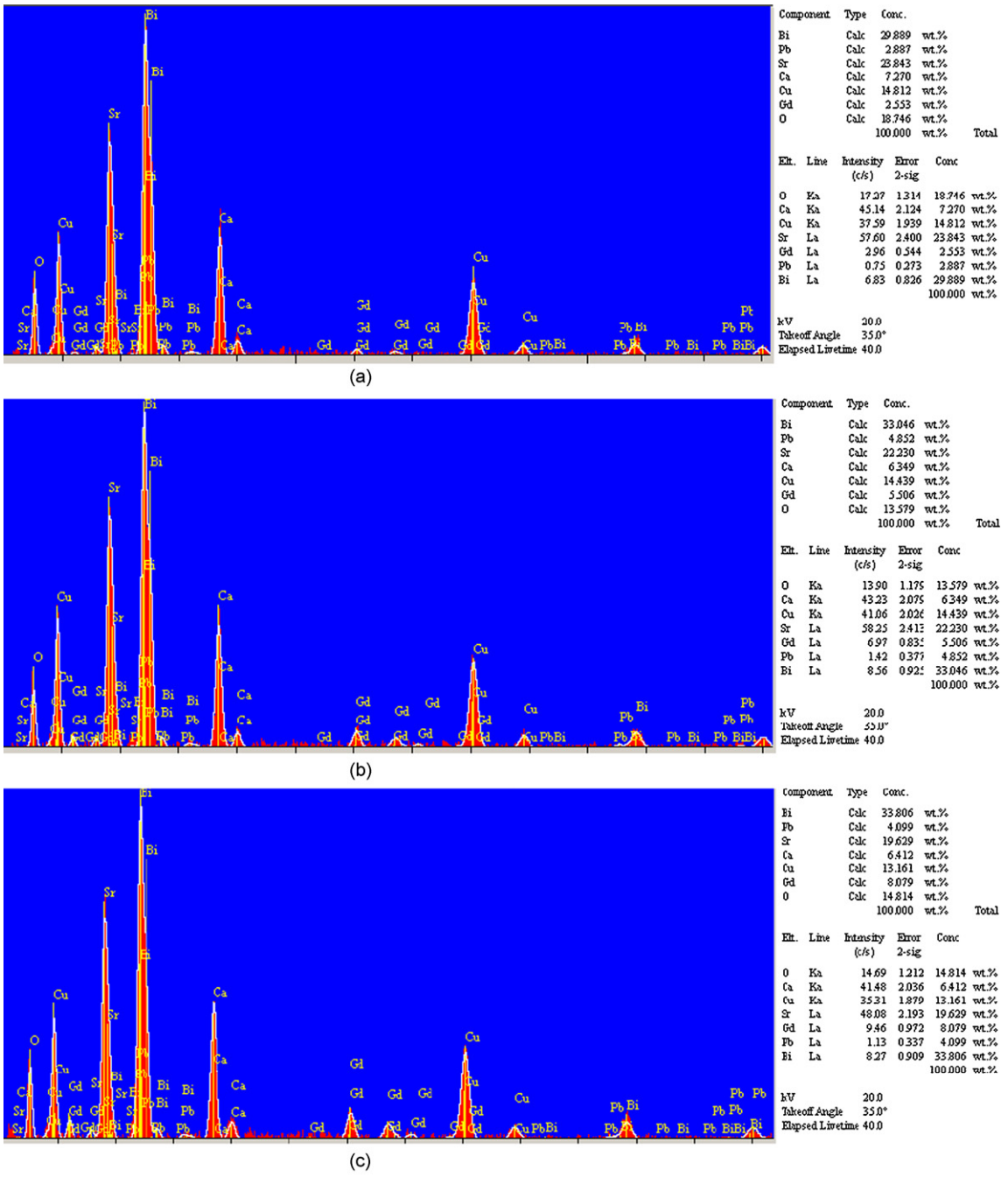

Fig. 3. EDS results of the Gd added samples (a) Gd1, (b) Gd3 and (c) Gd5.

There is a clear difference between the data of Gd0 and Gd-doped samples. The transition width of Gd0 is sharp and narrow while the transitions of Gd-doped samples broaden with increasing Gd content. The broadening of the transition indicates that Gd added samples have lower percentage of the high-T_c phase and weak-links between the grains compared to that of pure sample, which is consistent with XRD and SEM measurements. A double transition is observed in resistivity curve for the sample Gd5. This phenomenon could be attributed to the transition of weak-links at the grain boundaries and attests that the inter-grain region of this sample is different from those of the other samples. This result agrees well with the SEM observation in the present work. The extracted T_c and room temperature resistivity values are given in Table 1. It is found that T_c decreases from 105 K for Gd0 to 42 K for Gd5 while the room temperature resistivity increases from 2.456 mΩ cm for Gd0 to 11.639 mΩ cm for Gd5. The decrease in T_c is consistent with the results of microhardness results which indicate on overall degradation of the Bi-2223 phase with Gd-doping. Simon et al. [25] and Nanda Kishore et al. [26] have investigated the effect of Gd substitution in place of Ca in Bi(Pb)SrCaCuO and reported a decrease in T_c very similar to our findings. It might be possible that in our case, some of the added Gd reside in grain boundaries as indicated by an increase in the room temperature resistivity while the remaining ones could substitute the calcium or strontium in $Bi_{1.8}Pb_{0.35}Sr_{1.9}Ca_{2.1}Cu_3O_y$ [27].

We have also performed critical current density measurements at 77 K and J_c values for Gd0 and Gd1 samples are estimated to be 90 A/cm^2 and 10 A/cm^2, respectively. Since Gd3 and Gd5 samples

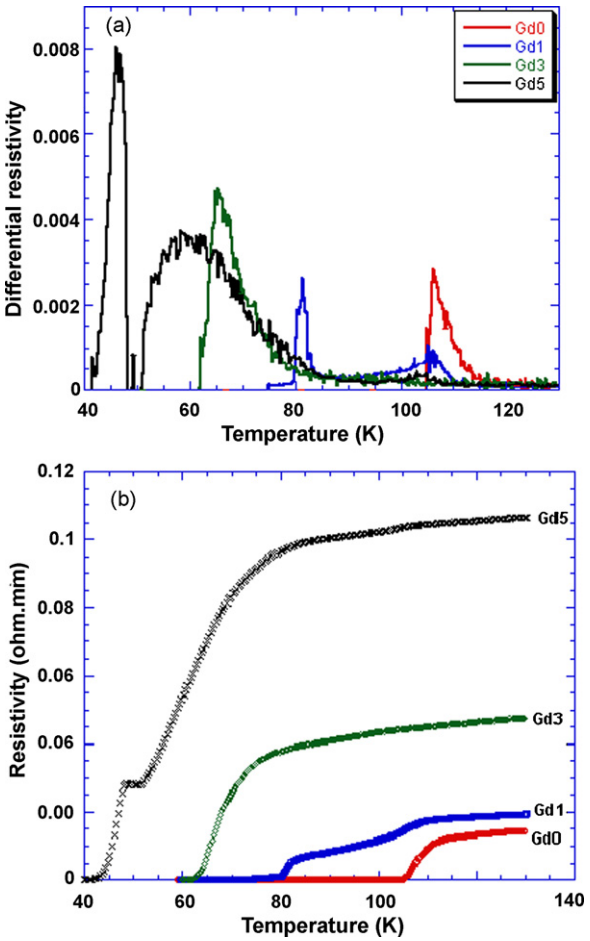

Fig. 4. (a) Derivative resistivity and (b) resistivity as a function of temperature curves for the Gd0, Gd1, Gd3, and Gd5 samples.

are not superconducting at 77 K, there is no data on J_c of them. As mentioned before, J_c decreases with increasing Gd content which might be caused by the decrease of grain size, random orientation of the grains, and weak-links caused by grain boundary regions modified by the presence of Gd atoms.

In summary, from the microstructure and transport measurements, we have found that Gd-doping of $Bi_{1.8}Pb_{0.35}Sr_{1.9}Ca_{2.1}Cu_3Gd_xO_y$ samples degrades the transition temperature, critical current density, grain connectivity, grain size and surface morphology of the samples. The effect of Gd addition might be two-fold; on the one hand it changes the properties of the grain boundaries, on the other substitute the Ca of Bi(Pb)–Sr–Ca–Cu–O and causes a decrease in T_c and J_c. Also, Gd-doping decreases the high-T_c phase fraction.

3.2. Microhardness and modelling

We have investigated the mechanical (microhardness, Young's modulus, yield strength and fracture toughness) properties of the same samples used in the present study and found that increase in Gd addition as well as the applied load would lead to a degradation of mechanical properties. Also a non-linear relation between the applied load and microhardness was observed in the same study [18]. In the present study, we would like to use a number of models to delineate the ISE behavior in Gd-doped samples.

We have done a series of hardness measurements on Gd0, Gd1, Gd3 and Gd5 samples using indentation loads in the range 0.245–2.94 N. The obtained data is plotted in Fig. 5 as the variation

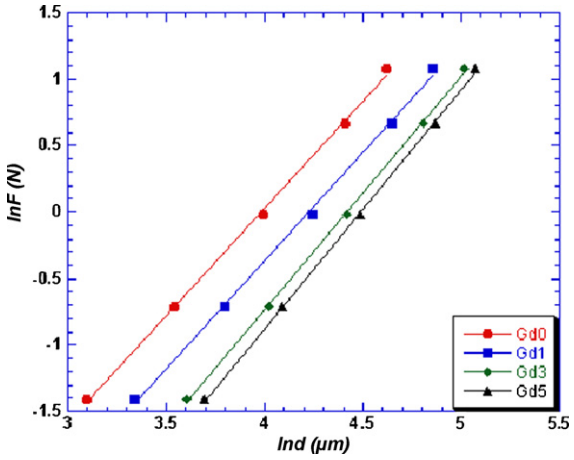

Fig. 5. Variation of applied load ln F with diagonal ln d for the samples.

Table 2
Best-fit results of experimental data according to Meyer's law.

Samples	Meyer number n	ln K (GPa)	Regression coefficient (R)
Gd0	1.623	−6.4586	0.99933
Gd1	1.631	−6.8924	0.99920
Gd3	1.761	−4.7777	0.99969
Gd5	1.796	−8.0553	0.99977

of ln F versus ln d. From previous work [18], we know that Vickers microhardness depends on the load. The variation of ln F versus ln d shows an excellent linear behavior and is fitted Meyer's law. The results of linearly regressed n, ln K and regression coefficient R are displayed in Table 2. As can be seen from the table, the fact that $R > 0.999$ for all the samples indicates that the linear fit is very good. Also we have found that when Gd content is increased, n increases while K decreases. However, the results indicate that for the present samples Kick's law is not valid because n is found to be less than 2. From Table 2, Meyer's law can explain the ISE behavior of our data qualitatively well, but the physical sense of the parameter K is still not well understood because its significance in the model is not very clear.

Next, we use the PSR model to analyze the load versus indentation data for the samples Gd0, Gd1, Gd3 and Gd5. The PSR model parameters K_1 and K_2 were obtained in our previous work [18]. These values and the R of the regression along with H_{PSR} of Eq. (6) are displayed in Table 3. We observe that K_1 and K_2 parameters decrease with increasing Gd content, which is similar to the case for the K of Meyer's model. The variation of microhardness as a function of indentation load for a variety of ceramic materials was investigated by Quinn and Quinn [12]. It was observed that such hardness–load curve shows distinct transition to a plateau of the constant hardness level and concluded that the plateau value of such curves correspond to the intrinsic hardness value of the material. In the present work, this plateau is reached at an applied load of 1.96 N for all the samples. It is obvious from Table 3 that the true microhardness value according to the PSR model (0.412 GPa)

Table 3
Best-fit results of experimental data according to PSR model.

Samples	K_1 (N/μm)	K_2 (GPa)	H_{PSR} (GPa)	R	H_v (GPa) in plateau region
Gd0	6.16	0.00022240	0.412	0.9990	0.534–0.538
Gd1	4.63	0.00013909	0.258	0.9991	0.330–0.333
Gd3	2.48	0.00011261	0.209	0.9992	0.242–0.243
Gd5	1.97	0.00010256	0.190	0.9990	0.215–0.216

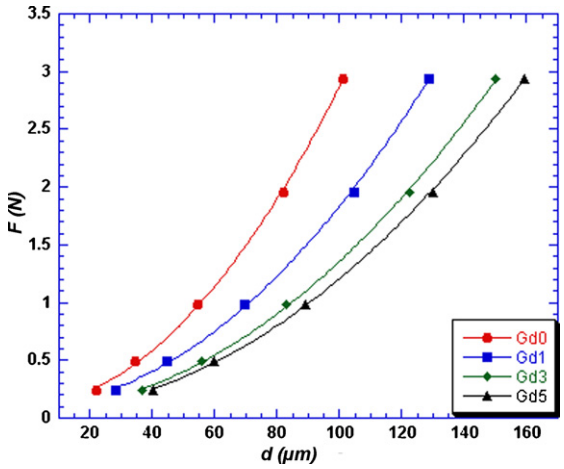

Fig. 6. Variation of applied load with the indentation diagonal length for the samples.

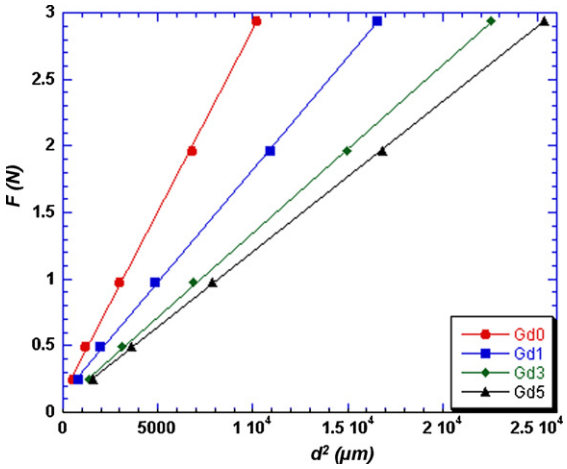

Fig. 7. Applied load versus the square of the impression semidiagonal length for the samples.

of Gd0 sample is lower than the hardness value in the saturated region (H_v = 0.534 GPa). This behavior is also observed in all the other samples (Gd1, Gd3, and Gd5). It was argued that the parameters of PSR model has a meaning and cannot be used to analyze ISE in nanoindentation regions for a large range of applied loads [15]. When examining the load dependence of the microhardness of materials measured in a wide range, it was found that the resultant F/d versus d curves show significant non-linearity [4,19] and Gong et al. [19] argued that the PSR model mentioned above may only be used to represent the experimental data in a narrower range of applied loads.

According to the MPSR model, the indentation load is related to the indentation diagonal length as in Eq. (7). Fig. 6 shows F versus d graph for our samples. From a conventional polynomial fit of the expression (Eq. (7)) to the data, the MPSR parameters K_3, K_4, K_5 and R of the fit were extracted for all the samples and tabulated in Table 4. The resulting true hardness is also computed using the same equation and is given in this table. It was found that the values of true hardness of the samples decreased with increasing the Gd content similar to the case for Meyer's and PSR models. As can be seen from Table 4, true microhardness value (0.477 GPa) of Gd0 sample calculated using MPSR model is still lower than the hardness result in the plateau region (H_v = 0.534 GPa). This behavior is also observed for all the samples (Gd1, Gd3, and Gd5) in this work. The value of true microhardness calculated using Eq. (6) is closer to the value of apparent microhardness in the plateau region than that of PSR model. On the other hand, as can be seen from the table, increasing Gd-doping decreases K_4, K_5, H_{MPSR} while its effect on K_3 seems to be non-monotonous; K_3 of Gd0 is 0.092. It increases to 0.096 for Gd1 but decreases to 0.061 for Gd3.

Finally, we use the model proposed by Hays and Kendall (HK) [11] to examine our data. The experimental F versus d^2 graph along with the least-square fit function are plotted in Fig. 7 and the best-fit parameters K_6 and $F_{0\,HK}$, the R of the fit, HK true hardness and plateau hardness values are displayed in Table 5. As can be seen from the table, the values of $F_{0\,HK}$ and K_6 of the samples decrease with increasing Gd content. Clearly, the present data for each sample shows an excellent linear relationship in HK approach and the regression coefficient of each sample is very high, $R > 0.9997$, implying that Eq. (8) provides a satisfactory description of the indentation data for the samples. The true hardness values estimated by HK approach (H_{HK} = 0.507 GPa) and the apparent hardness result of Gd0 sample in the plateau region (H_v = 0.534 GPa) are comparable. This behavior is also observed in the other samples (Gd1, Gd3 and Gd5) of this work. Based on the closeness of H_{HK} and H_v, one would speculate that among the models considered here, HK model has the highest success in according for the indentation data. The extracted values of $F_{0\,HK}$ were found to vary from 0.143 to 0.077 N. It means that the minimum load necessary to initiate permanent deformation for Gd5 is higher than 0.077 N. On the other hand, the estimated value of $F_{0\,HK}$ was generally found too large to be acceptable [15,28], which is consistent with our findings. Therefore, the HK approach is not convenient to estimate the value of $F_{0\,HK}$ of the samples.

As a summary of the results presented above, we have used four different empirical models to analyze the microindentation data on Gd-doped $Bi_{1.8}Pb_{0.35}Sr_{1.9}Ca_{2.1}Cu_3O_y$ samples. We have found that although each of the considered models might provide a satisfactory description of the relationship between the applied load and indentation diagonal length, they have different shortcomings in estimating the intrinsic hardness. As a result, one can conclude that indentation is a rather complex phenomenon that can be analyzed based on a single mechanism.

We consider the effect of Gd content and display the microhardness as a function of x for $Bi_{1.8}Pb_{0.35}Sr_{1.9}Ca_{2.1}Cu_3Gd_xO_y$ samples at various applied loads in Fig. 8. The microhardness value decreases non-linearly as x increases from 0 to 0.5. It is observed that the addition of Gd into $Bi_{1.8}Pb_{0.35}Sr_{1.9}Ca_{2.1}Cu_3O_y$ produces a softening effect in the investigated range (x = 0.1–0.5). This degradation is attributed to the formation of impurity phases and irregularities mainly distributed at the grain boundaries. This impurities and irregularities cause distortion of the bond strength, and conse-

Table 4
Best-fit results of experimental data according to MPSR model.

Samples	K_3 (N)	K_4 (N/μm)	K_5 (N/μm²)	(R)	H_{MPSR} (GPa)	Load dependent hardness (in plateau region) H_v (GPa)
Gd0	0.092	205.3×10^{-5}	25.7×10^{-5}	0.99971	0.477	0.534–0.538
Gd1	0.096	123.0×10^{-5}	16.2×10^{-5}	0.99980	0.300	0.330–0.333
Gd3	0.061	76.2×10^{-5}	12.2×10^{-5}	0.99990	0.226	0.242–0.243
Gd5	0.057	46.8×10^{-5}	11.0×10^{-5}	0.99994	0.204	0.215–0.216

Table 5
Best-fit results of experimental data according to HK model.

Samples	K_6 (GPa)	$F_{0\,HK}$ (N)	R	H_{HK} (GPa)	Load dependent hardness (in plateau region) H_v (GPa)
Gd0	27.3×10^{-5}	0.143	0.99966	0.507	0.534–0.538
Gd1	17.0×10^{-5}	0.135	0.99977	0.315	0.330–0.333
Gd3	12.6×10^{-5}	0.090	0.99988	0.234	0.242–0.243
Gd5	11.3×10^{-5}	0.077	0.99993	0.210	0.215–0.216

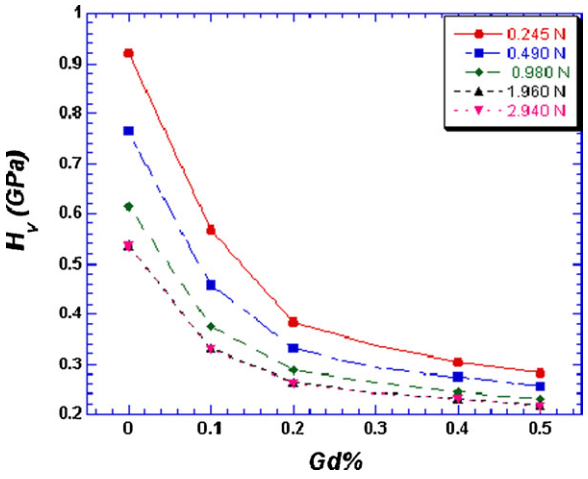

Fig. 8. The variation of apparent microhardness as a function of Gd content at different applied loads.

quently the apparent hardness of the specimen decreases [29,30]. This similar decrease in apparent hardness is revealed for the transition temperature in the present work.

4. Conclusions

We have presented the results of a detailed analysis of indentation study of Gd-doped $Bi_{1.8}Pb_{0.35}Sr_{1.9}Ca_{2.1}Cu_3Gd_xO_y$ superconducting ceramics. The study has emphasis on two aspects: i) Relation between hardness and applied load and its behavior for different doping levels. We have used four different empirical models to analyze the non-linear relation between the load and hardness and presented a comparison of the performance of the considered models. ii) We have used XRD, SEM, dc resistivity and transport J_c measurements to characterize crystal structure, morphology, T_c, room temperature resistivity and critical current density as a function of temperature and doping level. The conclusions based on the results can be summarized as follows:

- Gd addition is found to decrease the hardness of the samples. This degradation is due to increasing voids, impurity phase segregation and the modification of the grain boundaries which are also observed in SEM images and XRD patterns.
- Among the four empirical models used to analyze the load versus indentation data, we have found that HK model is the best one for obtaining a hardness value which is close to the intrinsic hardness. But, the minimum applied load to produce an indentation, $F_{0\,HK}$, found in this model seems to be too high to be acceptable.

Acknowledgements

Author wants to thank Dr. Resul Eryigit for interpretation of data and writing the paper. This work is supported partly by the Scientific and Technological Council of Turkey (Project No: 104T325) and partly by the Turkish State Planning Organization (DPT) (Project No: 2004K120200).

References

[1] J. Gong, J. Wu, Z. Guan, J. Eur. Ceram. Soc. 19 (1999) 2625.
[2] J. Gong, J. Wu, Z. Guan, Mater. Lett. 38 (1999) 197.
[3] S.M. Khalil, J. Phys. Chem. Solids 62 (2001) 457.
[4] M. Yilmazlar, H.A. Cetinkara, M. Nursoy, O. Ozturk, C. Terzioglu, Physica C 442 (2006) 101.
[5] S.M. Khalil, J. Phys. Chem. Solids 64 (2003) 855.
[6] S.M. Khalil, Smart Mater. Struct. 14 (2005) 804.
[7] M. Yilmazlar, O. Ozturk, O. Gorur, I. Belenli, C. Terzioglu, Supercond. Sci. Technol. 20 (2007) 365.
[8] U. Kolemen, O. Uzun, M.A. Aksan, N. Guclu, E. Yakinci, J. Alloys Compd. 415 (2006) 294.
[9] W. Zewen, J. Wanqi, Mater. Sci. Eng. A 452–453 (2007) 508.
[10] H. Li, R.C. Bradt, J. Mater. Sci. 28 (1993) 917.
[11] C. Hays, E.G. Kendall, Metallography 6 (4) (1973) 275.
[12] J.B. Quinn, G.D. Quinn, J. Mater. Sci. 32 (1997) 4331.
[13] B.W. Mott, Microindentation Hardness Testing, vol. 9, Butterworths, London, 1956.
[14] A.A. Elmustafa, D.S. Stone, J. Mech. Phys. Solids 51 (2003) 357.
[15] Z. Peng, J. Gong, H. Miao, J. Eur. Ceram. Soc. 24 (2004) 2193.
[16] B.R. Lawn, V.R. Howes, J. Mater. Sci. 16 (1981) 2745.
[17] H.J. Weiss, Phys. Status Solidi 99 (1987) 491.
[18] H. Aydin, O. Cakiroglu, M. Nursoy, C. Terzioglu, Chin. J. Phys. 47 (2) (2009) 192.
[19] J.H. Gong, J.J. Wu, Z.D. Guam, J. Mater. Sci. Lett. 17 (1998) 473.
[20] C. Terzioglu, O. Ozturk, A. Kilic, A. Gencer, I. Belenli, Physica C 434 (2006) 153.
[21] O. Görür, C. Terzioglu, A. Varilci, M. Altunbaş, Supercond. Sci. Technol. 18 (2005) 1233.
[22] C. Terzioglu, M. Yilmazlar, O. Ozturk, E. Yanmaz, Physica C 423 (2005) 119.
[23] C. Terzioglu, H. Aydın, O. Ozturk, E. Bekiroglu, I. Belenli, Physica B 403 (2008) 3354.
[24] A. Amira, F. Bouaicha, N. Boussouf, M.F. Mosbah, Solid-State Sci. 12 (2010) 699.
[25] S. Simon, G. Ilonca, I. Barbur, Physica &LPKT;Utrecht&RPKT; 162/164C (1989) 1289.
[26] K. Nanda Kishore, S. Satyavathi, M. Muralidhar, V. Hari Babu, O. Pena, M. Sergent, F. Beniere, Phys. Status Solidi A 143 (1994) 101.
[27] R.P. Aloysius, P. Guruswamy, U. Syasmaprasad, Physica C 426–431 (2005) 556.
[28] M. Nursoy, M. Yilmazlar, C. Terzioglu, I. Belenli, J. Alloys Compd. 459 (2008) 399.
[29] C. Veerender, V.R. Dumke, M. Nagabhooshanam, Phys. Status Solidi A 144 (1994) 299.
[30] M. Muralidhar, K.N. Reddy, V.H. Babu, Phys. Status Solidi A 126 (1991) 115.